Exploring Beamforming Performance Versus Complexity in Reconfigurable Aperture Antennas

Rashid Mehmood and Jon W. Wallace
Jacobs University Bremen
Campus Ring 1, 28759 Bremen, Germany
E-mail: r.mehmood@ieee.org, wall@ieee.org

***Abstract*—Reconfigurable aperture (RECAP) antennas consist of a regular array of reconfigurable elements confined to an aperture, representing a generalization of the reconfigurable antenna concept. RECAPs have the potential of supporting operations like beamforming, null steering, interference suppression, adaptive matching, and frequency and bandwidth agility in a single aperture. Although very complex RECAP structures theoretically have performance that is only limited by the physical extent of the aperture, high complexity is impractical due to increased loss, biasing difficulties, and system cost. This work reviews the RECAP antenna concept and focuses on the role of performance bounds imposed by limited complexity in practical RECAP structures. This initial effort studies empirical bounds on beamforming performance observed from detailed simulation of two idealized RECAP structures: (i) a 5×5 parasitic dipole array, and (ii) a 8×8 planar configuration of reactively connected patches. Performance bounds for limited complexity are identified, indicating the number of elements per wavelength and the states per reconfigurable element that are needed to capture most of the available performance.**

***Index Terms*—Antenna arrays, reconfigurable antennas, beam steering, genetic algorithms**

I. Introduction

Antenna systems and algorithms that can effectively adapt their operation to changing needs and environmental conditions have been the subject of intense research over the past few decades. The need of such architectures has been especially apparent in the realm of wireless communications, due to a dramatic rise in services, applications, and users coupled with the scarcity and high cost of radio-frequency (RF) spectrum. Adaptive antennas mitigate this problem by providing high spectral efficiency, allowing higher data rates or more users to be supported on fixed available spectrum.

Smart antennas represent perhaps the most flexible solution, where physical antenna elements are simple transducers, whose signals are digitized and jointly processed by powerful digital signal processing (DSP) architectures. Smart antennas can support diversity, beamforming, interference suppression, and spatial multiplexing, thus maximizing user performance for the channels and conditions that are present. Although smart antennas are a very powerful concept, one concern is the cost associated with the multiple RF chains and additional DSP resources, which can limit their use in many practical applications.

Reconfigurable antennas take the opposite approach, which is to put additional complexity in the transducer [1], allowing similar operations to be performed as smart antennas, such as beam steering [2] and pattern null creation [3], but with only a single RF chain and modest DSP resources. Reconfigurability is achieved by employing semiconductor switches fabricated with PIN diodes or FETs, MEMs switches, or tunable reactances such as varactor diodes. In some cases, higher performance is possible with reconfigurable antennas, since the signal is processed in the analog domain before amplifiers and analog-to-digitial (A/D) conversion that introduce noise, quantization, and limited dynamic range. Further, reconfigurable antennas can support operations such as frequency agility and adaptive matching that are not possible in the digital domain [4], [5].

The switched parasitic array, introduced as early as [6], serves a similar purpose as a reconfigurable antenna, where one or relatively few elements are connected to active RF circuitry, while the bulk of the antennas are connected to switched reactive loads having two possible states. By changing the state of the loads, the effective pattern of the array is altered. For closely spaced antenna elements exhibiting mutual coupling, the state of the switched parasitic loads also modifies the active antenna match. Switch parasitic arrays support beamsteering [7] and diversity [8].

The reconfigurable aperture antenna (RECAP) [9], [10] is similar to a rectangular switched parasitic array, consisting of a regular array of reconfigurable elements (REs) whose state can be electronically controlled. When the degree of reconfigurability of the RECAP is large and loss of the REs sufficiently low, RECAPs have the potential to dynamically synthesize antenna parameters, constrained only by the physical aperture of the device. A basic problem with RECAPs is the need for efficient search algorithms to find a near-optimal state of the REs, typically requiring a genetic algorithm. For this reason, concepts similar to the RECAP have been described as evolvable antennas [11] and self-structuring antennas [12].

We believe that the RECAP is an intriguing concept that deserves significant attention, since it potentially provides generalized reconfigurability in the analog antenna domain, similar to what is provided by programmable logic devices in the digital domain. Although the idea is already well established, there are many outstanding questions that must be addressed to understand the limits of the technology and make it practical for real applications.

Our present research studies the role of complexity in RECAP antennas, where complexity consists of the number of reconfigurable elements (N_{RE}) and number of reconfig-

urable states (N_{RS}) per element. This work addresses several important questions: What level of complexity is required to fully exploit the degrees of freedom of a given aperture? For bounded complexity, can a bound on the performance also be clearly identified? Do reconfigurable elements and states per element play an equally important role in complexity constrained performance? Is the role of complexity significantly altered by topological differences? Does complexity impact the convergence and efficiency of search algorithms for the REs?

To provide some initial answers to these questions, this paper studies the beamforming performance of two idealized RECAP structures, each confined to a $1\lambda\times1\lambda$ aperture. The first antenna is a 5×5 loaded dipole array. The second structure is a planar 8×8 array of interconnected patch antennas. In each case, an efficient full-wave/network-analysis approach is used to simulate the the antenna, coupled with a genetic algorithm (GA) to find adequate solutions for the state of the REs to steer a beam in a specified direction. The average performance over many runs of the GA is then used to derive empirical bounds on the performance for a given level of complexity.

The remainder of the paper is organized as follows: Section II explains the simulation method that was used to study RECAPs, followed by Sections III and IV that study the dipole array and planar antenna, respectively. Section V concludes the paper.

II. Simulation of RECAP Antennas

This section describes the efficient hybrid simulation technique that was used to analyze the RECAP antennas, the method for studying performance versus complexity, as well as the genetic algorithm thas was employed to find good solutions for the REs.

A. Hybrid Full-Wave/Network Analysis of RECAP Antennas

Full-wave simulation of RECAP antennas for all required configurations of the REs is computationally expensive, since many thousands of trials are typically required. Therefore an efficient simulation method is adopted that consists of full-wave simulation of the unloaded array, combined with network analysis to find network characteristics and radiation patterns for arbitrary loading.

Figure 1 depicts a generic RECAP antenna consisting of a single active feed port (Port 1) and additional ports that are terminated with reconfigurable elements (Ports 2-N). A complete characterization of the antenna is possible by running N full-wave simulations, where for the kth simulation, a source is used to excite the kth port and other ports are terminated with a convenient load. By storing the vector of voltages $\mathbf{v}^{(k)}$ and currents $\mathbf{i}^{(k)}$ present at all ports as well as far-fields $\mathbf{E}_k(\theta,\phi)$ for each of the N simulations, input impedance and the radiation pattern for arbitrary loading can be computed very efficiently.

For the dipole array considered in Section III, the Numerical Electromagnetics Code (NEC) was used, where a unit voltage source is placed on the terminals of the excited antenna, and the other antennas are modeled as a single wire with no gap

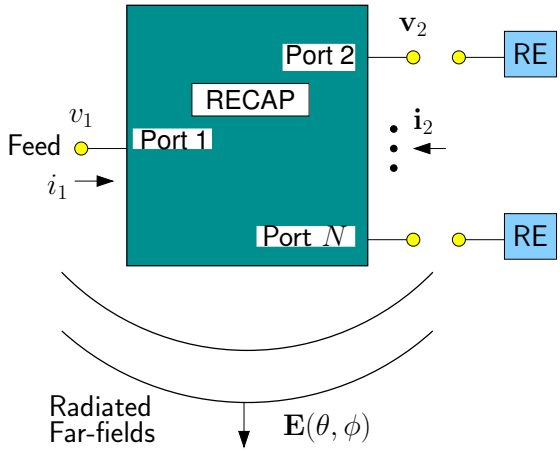

Fig. 1. Characterization of a generic RECAP antenna

(short-circuit). In this case, an admittance formulation is most convenient, since for the kth excitation $v_\ell^{(k)} = \delta_{k\ell}$, where $\delta_{k\ell}$ is the Kronecker delta function, so that $\mathbf{i}^{(k)}$ gives the kth column of the impedance matrix $\mathbf{Y}$ and the far-fields give the short-circuit radiation pattern of the the kth element or $\mathbf{E}_k^{\rm sc}(\theta,\phi)$.

Network analysis is used to compute the input impedance and radiation pattern of the antenna when one port is the feed and the other ports are terminated with REs as follows. Using the arrangement in Figure 1, we have $\mathbf{i} = \mathbf{Y}\mathbf{v}$, or

$$\begin{bmatrix} i_1 \\ \mathbf{i}_2 \end{bmatrix} = \begin{bmatrix} y_{11} & \mathbf{y}_{12} \\ \mathbf{y}_{21} & \mathbf{Y}_{22} \end{bmatrix} \begin{bmatrix} v_1 \\ \mathbf{v}_2 \end{bmatrix}, \tag{1}$$

where i_1 and v_1 are the scalar current and voltage on the feed, $\mathbf{i}_2$ and $\mathbf{v}_2$ are vectors of currents and voltages for the ports to be terminated with reconfigurable elements, and $\mathbf{Y}$ has been partitioned appropriately. Terminating port $k+1$ with admittance $y_{L,k}$, $k = 1,\ldots,N-1$, we have $\mathbf{i}_2 = -\mathbf{Y}_L\mathbf{v}_2$, where $\mathbf{Y}_L$ is a diagonal matrix with $Y_{L,kk} = y_{L,k}$. Combined with (1), we have

$$\mathbf{v}_2 = -(\mathbf{Y}_{22} + \mathbf{Y}_L)^{-1}\mathbf{y}_{21}v_1, \tag{2}$$

and

$$i_1 = \underbrace{y_{11} - \mathbf{y}_{12}(\mathbf{Y}_L + \mathbf{Y}_{22})^{-1}\mathbf{y}_{21}}_{y_{\rm in}} v_1, \tag{3}$$

where $y_{\rm in}$ is the input admittance looking into the feed for the given termination at the REs. The realized radiation pattern of the array for feed voltage v_1 is found using superposition as

$$\mathbf{E}(\theta,\phi) = \sum_{k=1}^{N} v_k \mathbf{E}_k^{\rm sc}(\theta,\phi), \tag{4}$$

where voltages at the REs are found with (2).

The reflection coefficient looking into the feed will also be considered, given by $\Gamma = (z_{\rm in} - Z_0)/(z_{\rm in} + Z_0)$, where Z_0 is a normalizing impedance, which is taken to be the internal impedance of the source driving the antenna and $z_{\rm in} = 1/y_{\rm in}$. The network-analysis technique was tested

extensively by considering several configurations directly with full-wave simulations and comparing to results from network analysis. Virtually exact agreement was possible in this work by making the gaps of the physical ports small enough, such that the REs act very close to lumped elements with no radiation. Distributed REs could still be accommodated with this hybrid technique, but this would require full-wave simulations of the REs, allowing their radiated fields to be included in (4).

For the planar patch array, full-wave simulation was performed with a custom FDTD code, where unit current excitation on the excited port and open-circuit terminations for the non-excited ports was used. In this case an impedance formulation is more convenient, which is exactly analogous to the admittance formulation, but $\mathbf{i}$ and $\mathbf{v}$ change roles. In this case the kth simulation yields the vector of voltages $\mathbf{v}^{(k)}$ which is also the kth column of the impedance matrix $\mathbf{Z}$ and the farfields give the kth open-circuit radiation pattern $\mathbf{E}_k^{\text{oc}}(\theta, \phi)$.

Arranging the ports as before, the radiation pattern for arbitrary values of the REs is given by superposition, or

$$\mathbf{E}(\theta, \phi) = \sum_{k=1}^{N} i_k \mathbf{E}_k^{\text{oc}}(\theta, \phi), \tag{5}$$

and input impedance is given by

$$z_{\text{in}} = z_{11} - \mathbf{z}_{12}(\mathbf{Z}_L + \mathbf{Z}_{22})^{-1}\mathbf{z}_{21}. \tag{6}$$

As with the admittance formulation, network analysis was checked by running full-wave simulations for several specific configurations of the REs and near exact agreement was obtained.

B. Genetic Algorithm

Due to the complicated relationship of RECAP operation on the state of the REs, finding the set of REs to achieve the required beamforming performance is a non-convex optimization, requiring some kind of global search. Although an exhaustive search would find the optimal solution, even with the hybrid simulation strategy the computational burden is too high for moderate and large values of N_{RE} and N_{RS}. In this work, we applied a genetic algorithm (GA) to find good solutions for the states of the REs. Although not guaranteed to provide optimal performance, we feel that studying the behavior of good (but sub-optimal) solutions with respect to complexity is a useful first step.

The GA operates on a total population size of $N_P = 500$ *individuals*, where a single individual is represented as an $N_{RE}\times 1$ vector containing the admittances/impedances of the REs. The GA is initialized by considering $4N_P$ individuals chosen randomly from the whole population space, computing the fitness (beamforming performance) of each individual, and retaining the best $N_K = 100$ individuals. This random search phase is repeat 10 times, and the N_K best individuals are used to start the GA. Each iteration of the GA then proceeds by combining the N_K best solutions to generate $N_P - N_K$ new individuals using random cross-overs and mutations. The individuals are sorted by fitness, the N_K best solutions are retained, and the process repeats. If the GA reaches a stage when there is no significant improvement observed in the best solution for 10 iterations of GA, the best solution is stored and the GA is restarted with a new random population.

The performance of the genetic algorithm has been partially checked by considering exhaustive searches for lower RECAP complexity and multiple simplex searches for higher complexity, suggesting that the GA is finds near-optimal solutions, adequate for the goals of this study.

C. Performance vs. Increasing Complexity

RECAP complexity is defined in this paper in terms of the number of reconfigurable elements (N_{RE}) and the number of possible reconfigurable states (RSs) for each of those elements (N_{RS}). One can consider the total complexity of the antenna to be the number of bits that are needed to describe the complete state of the stucture, which is $\log_2({N_{RS}}^{N_{RE}}) = N_{RE}\log_2(N_{RS})$. For both types of antennas, simulations were run for all combinations of a set of possible N_{RE} and N_{RS} values, where the goal is to see the effect of complexity on convergence of the genetic algorithm, to identify where the onset of diminishing returns with increasing complexity occurs, and to determine whether complexity in terms of N_{RE} or N_{RS} is more significant.

The REs are terminated with loads chosen from a discrete set of N_{RS} impedance or admittance values. In this work we have assumed that REs consist of varactor diodes (continuously variable capacitances), where the phase of the input reflection coefficient can be varied between 0° and -180°. Since the peak performance may depend on the specific set of N_{RS} reconfigurable states that are allowed, careful consideration is required for each of the simulated RECAPs.

III. Dipole Array

The dipole array analyzed in this work is a 5×5 square dipole array constrained to a $1\lambda\times 1\lambda$ area as shown in Figure 2, which was taken from the Numerical Electromagnetics Code (NEC) software used to simulate the array. Each of the half wave dipoles considered here have wire diameter 0.015λ with 0.25λ inter-element spacing, where 21 segments per dipole were used in the NEC simulations. The differential feed point is chosen to be at the center dipole.

Increasing complexity in the number of reconfigurable states per RE was studied by considering the values $N_{RS} = [2\ 4\ 8\ 16\ 32]$. In order to study performance with respect to increasing N_{RE}, the values $N_{RE} = [4\ 8\ 16\ 24]$ were considered and corresponding configurations are shown in Figure 3, where the goal was to fill the aperture as uniformly as possible with the N_{RE} elements (and feed) and maintain a symmetric structure. For each case, only N_{RE} of the parasitic antennas are terminated in a reconfigurable element (denoted with filled circles), while the the others are open circuited (zero admittance). This strategy was chosen instead of removing the unterminated parasitic elements completely, since simulation time is dramatically reduced, and observed

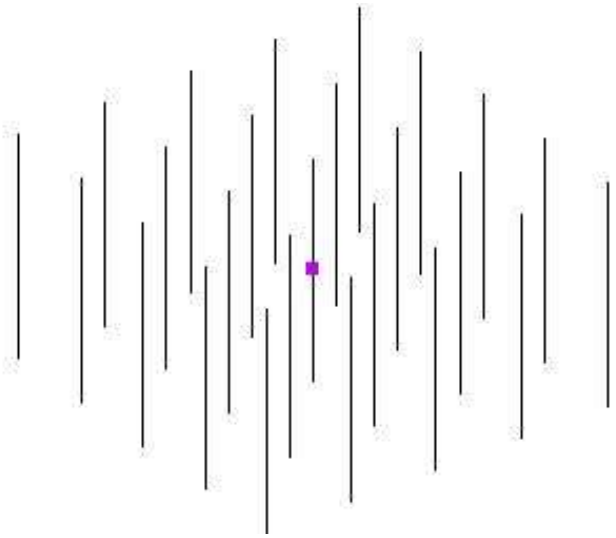

Fig. 2. Perspective view of dipole array RECAP

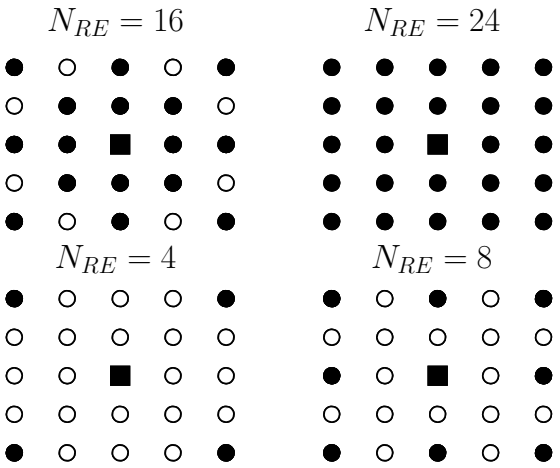

Fig. 3. Top-view of dipole array RECAP consisting of a 5×5 array, where N_{RE} elements are terminated with reconfigurable elements (the filled circles) and the center element marked by square is the feed

changes in performance are due to the REs alone and not due to changes in the array structure.

We have found through simulation of many random sets of allowed RSs as well as simulations with arbitrary continuous phase of input reflection coefficient that the optimal assignment appears to be nearly uniform. Hence the reconfigurable states are chosen such that the phase of input reflection coefficient is uniformly spaced on the allowed interval of $[-180°, 0°]$.

Figure 4 depicts the final GA solution for the radiation pattern of the antenna for a beam steered to $\phi = 171°$ for different values of N_{RS} for $N_{RE} = 24$ elements.

A. Performance Criterion

The beamforming performance goal considered for the parasitic array was to maximize the fraction of input power

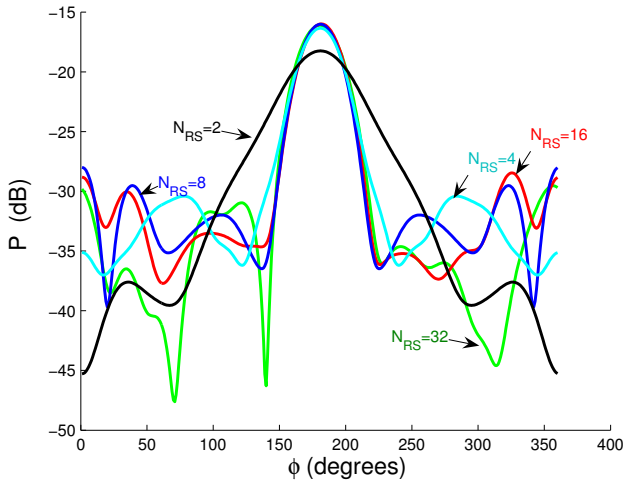

Fig. 4. Radiation patterns of the dipole array for final GA solutions with $N_{RE} = 24$ and varying N_{RS}. The main beam is specified to be at $\phi = 171°$.

radiated into a given sector in the azimuthal (xy) plane, or

$$P_{\text{beam}} = \max_{\mathbf{Y}_L}(1 - |\Gamma|^2)\frac{\sum_{n=n_0-N_B/2}^{n_0+N_B/2}|E_\phi(\phi_n, \theta = 90)|^2}{\sum_{n=1}^{N_A}|E_\phi(\phi_n, \theta = 90)|^2}, \tag{7}$$

where azimuth is sampled with $\Delta\phi = 2\pi/N_A$, $\phi_n = n\Delta\phi$, n_0 is the desired direction index for the main beam, the main beam occupies indices $n \in [n_0 - N_B/2, n_0 + N_B/2]$, and the two-sided beamwidth is $W = 2N_B\Delta\phi$. In the simulations that follow, we chose $N_A = 360$ sample angles, main beams at $n_0 = 60, 70, 80, 90$, and beamwidth $W = 40°$. Since the structure under consideration as well as reconfigurable element selection is symmetric, the small set of main beam angles is representative of the overall behavior of the structure for the whole 360° sweep of ϕ.

B. Representative Results

The convergence of genetic algorithm for the dipole array for a fixed number of N_{RE} and increasing N_{RS} is shown in Figure 5(a), where the curves are averaged over scan angles ranging from $60° - 90°$ in $10°$ increments. Three basic regions are typically seen in these convergence plots. The first region shows the random search, followed by a dramatic increase in fitness obtained from the GA. The last region shows convergence to a (local) maximum of the GA, where diminishing returns are seen with additional iterations.

The plot suggests that increased complexity does not affect the initial convergence of the algorithm significantly, but rather just increases the final performance of the solution. Also illustrated is a point of diminishing returns with increasing states, where for 32 states, there is virtually no benefit compared to 16 states.

Figure 5(b) shows the convergence of the GA for increasing N_{RE} for a fixed number of N_{RS}, indicating that additional complexity does not degrade the ability to find good solutions with the GA. Also, a level of diminishing returns is seen at 24

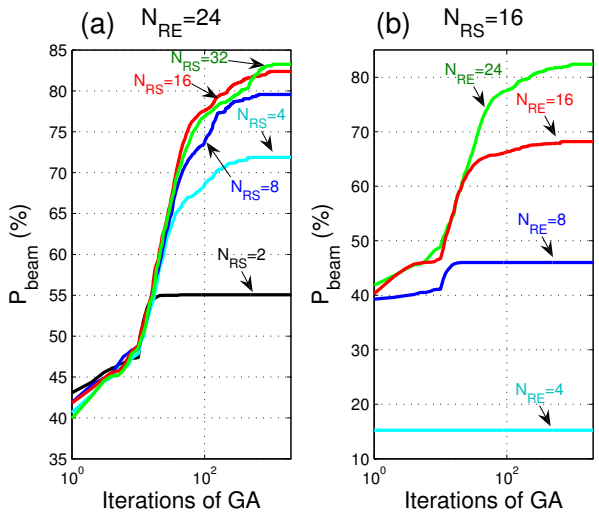

Fig. 5. Convergence of the genetic algorithm (a) $N_{RE} = 24$ and varying N_{RS} and (b) $N_{RS} = 16$ and varying N_{RE} for the dipole array.

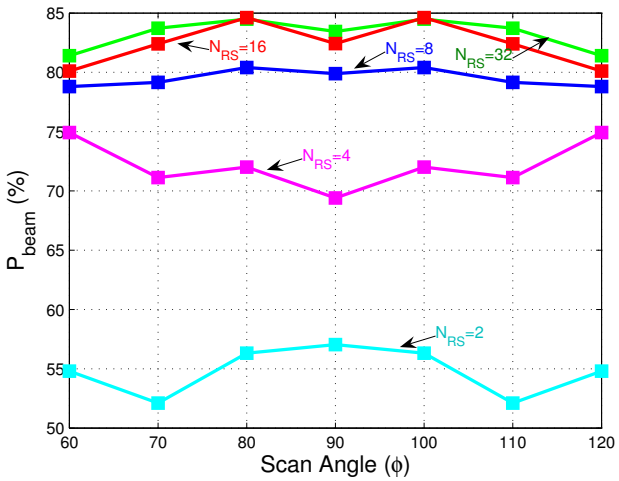

Fig. 6. Percentage input power focused in a 40° azimuthal sector for different mean angles as a function of the number of reconfigurable states N_{RS} for $N_{RE} = 24$ for the dipole array

REs, corresponding to 5 elements per wavelength. However, it is likely that slightly more dipoles (and REs) are needed to see the full saturation as observed with the RSs.

Figure 6 depicts the fraction of input power radiated into a 40° sector centered at the specified angles as a function of the number of reconfigurable states for $N_{RE} = 24$. It can be clearly observed that as the number of states per element increases, the amount of power that can be focused in a given direction also increases. Also apparent are diminishing returns in the performance near $N_{RS} = 8$, where addtional complexity is not very beneficial.

Figure 7 shows the average value of percentage power in main beam obtained for all combinations of N_{RE} and N_{RS}. The results indicate that for a given value of N_{RE}, having more than $N_{RS} = 8$ states is not very beneficial. Beamforming

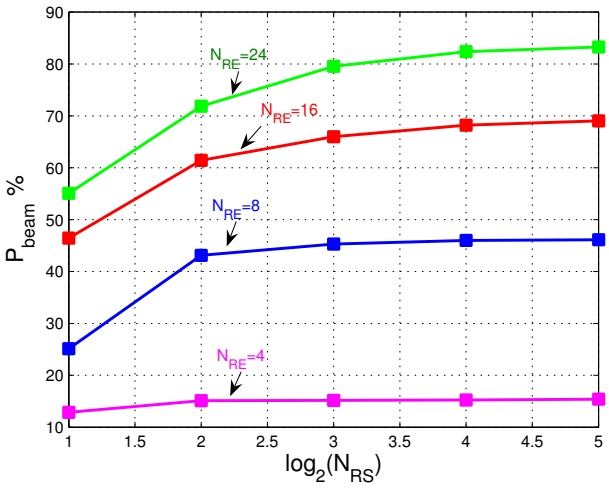

Fig. 7. Beamforming fitness for varying N_{RE} and N_{RS} for the dipole array

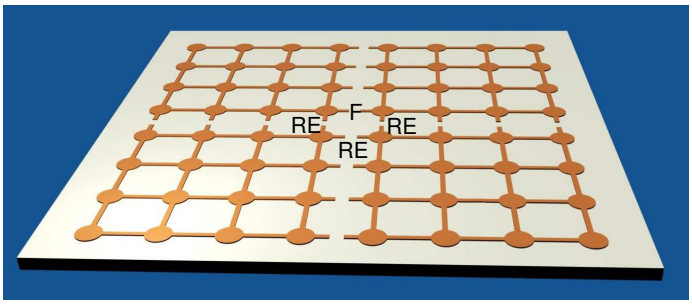

Fig. 8. Planar patch array RECAP for $N_E = 4$ logical elements, with $N_{RE} = 3$ reconfigurable elements (RE) and one feed (F)

performance increases steadily with increasing values of N_{RE}, where some saturation is seen after $N_{RE} = 16$. Note that when the number of elements in the aperture is small, doubling N_{RE} is more beneficial than doubling the exponent of N_{RS}, although each of these operations doubles the total complexity of the antenna. The higher importance of N_{RE} is reasonable, since for small N_{RE}, the aperture is likely to be undersampled and all spatial degrees of freedom are not yet exploited.

IV. Planar Patch Array

The planar patch array analyzed in this work is a 8×8 structure constrained to a $1\lambda\times1\lambda$ area as shown in Figure 8. The structure consists of circular patches connected with each other using transmission lines. Patches considered in this work have a radius of 0.038λ and are interconnected with transmission lines having length of 0.056λ and width of 0.015λ. Note that unlike normal patch antennas that are approximately $\lambda/2$ and have a ground plane underneath, this structure is just a single plane with individual patches that are small compared to the operational wavelength. The differential feed used in this case is approximately in the middle of the structure as shown in Figure 8. The RECAP was simulated with full-wave FDTD simulations and the impedance formulation for network

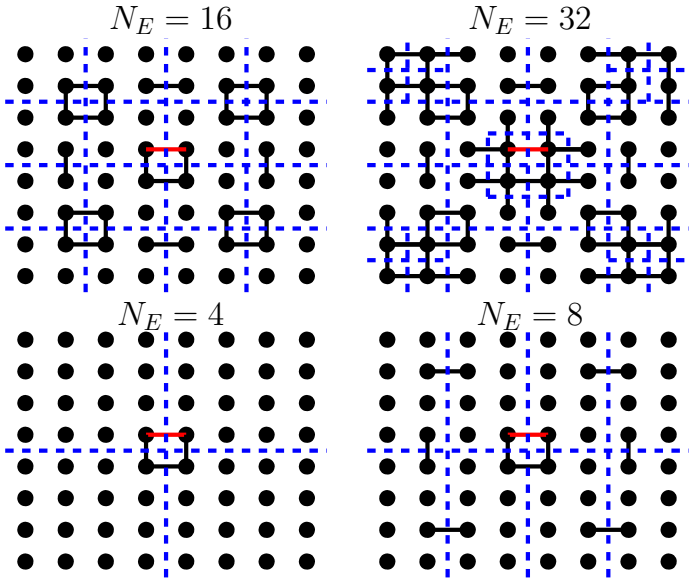

Fig. 9. Top-view of planar patch array RECAP consisting of 8×8 patches, where N_E logical elements are separated from each (dashed lines). Solid black lines show the location of an RE and the solid red line is the feed

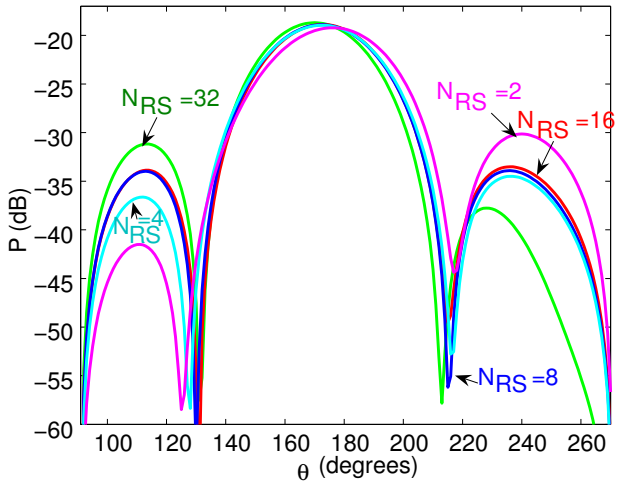

Fig. 10. Fraction of radiation power for $N_E = 64$ with varying N_{RS} for main beam at $\phi = 171°$ for planar patch array

analysis described in Section II-A. Also note that the GA used for the planar patch array was nearly identical to that of the parasitic array, with the exception that crossover and mutation probabilities needed to be tuned to obtain the best convergence.

A. *Performance Analysis with Increasing Complexity*

Similar to the dipole array, the performance goal here was to maximize the amount of input power radiated into a sector in the xz plane or

$$P_{\text{beam}} = \max_{\mathbf{Z}_L}(1-|\Gamma|^2)\frac{\sum_{n=n_0-N_B/2}^{n_0+N_B/2}|E_\theta(\theta_n,\phi=0)|^2}{\sum_{n=1}^{N_A}|E_\theta(\theta_n,\phi=0)|^2}, \quad (8)$$

where elevation is sampled with $\Delta\theta = 2\pi/N_A$, $\theta_n = n\Delta\theta$, n_0 is the desired direction index for the main beam, the main beam occupies indices $n \in [n_0 - N_B/2, n_0 + N_B/2]$, and the two-sided beamwidth is $W = 2N_B\Delta\theta$. In the simulations that follow, we chose $N_A = 180$ sample angles, main beams at $n_0 = 141, 161, 171, 181$, and beamwidth $W = 40°$.

Fixing the complexity in terms of the N_{RE} was not as straightforward for the planar patch array, since the elements are interconnected and REs can only be placed at these interconnection points. Figure 9 depicts schematically how the full grid is divided into N_E logical "elements" (regions of permanently connected patches) that are then connected by REs. In this figure, patches separated by dashed lines are always disconnected, while a solid black line between patches indicates an RE. The solid red line near the center of the structure indicates the active feed point. Patches with blank space between them in the figure are always conncted with a short circuit.

The number of logical elements considered was $N_E = [4\ 8\ 16\ 32\ 64]$, corrpsonding to $N_{RE} = [3\ 9\ 23\ 55\ 111]$ reconfigurable elements, respectively. Figure 8 shows the case for $N_E = 4$ for easier visualization. As with the parasitic array, the configurations for the different N_{RE} have been chosen to try to make the REs distributed as uniformly as possible over the antenna, while maintaining a symmetric structure.

As with the dipole array, the REs for the planar antenna are continuously variable capacitiances having a reflection coefficient phase in the interval $[-180°, 0°]$. However, instead of using a fixed set of impedance values for the set of RSs for all GA runs, the set was chosen randomly and uniform on $[-180°, 0°]$ for each run of the GA. Since more investigation is needed to determine a good set of RSs that works well for all values of N_E, this random assignment was done in this initial study to avoid unwanted bias due to a poor choice of the RSs for a given level of N_E. Figure 10 depicts the final GA solution for the radiation pattern of the antenna for a beam steered to $\phi = 171°$ for different values of N_{RS} for $N_E = 64$ elements.

Figure 11(a) shows the convergence of the GA for $N_E = 16$ and varying N_{RS}. Similar to the dipole array, we clearly see diminishing returns in the final performance for $N_{RS} = 8, 16$ and 32 RSs. Although for these higher RS values the added complexity does not increase the performance of the final solution, the convergence to that solution happens much more quickly with higher complexity. This suggests that for certain RECAPs, added complexity in N_{RS} may be beneficial for fast convergence of the search algorithm.

Figure 11(b) shows the convergence of GA for $N_{RS} = 32$ and increasing N_E. Diminishing returns in the performance of the final solution is seen for increasing N_E. As with N_{RS} we see that even when final performance is basically saturated, added complexity in terms of N_E can be beneficial in terms of providing higher performance with fewer GA iterations (faster convergence).

Figure 12 shows the average value of percentage power in main beam obtained for all combinations of N_E and N_{RS}

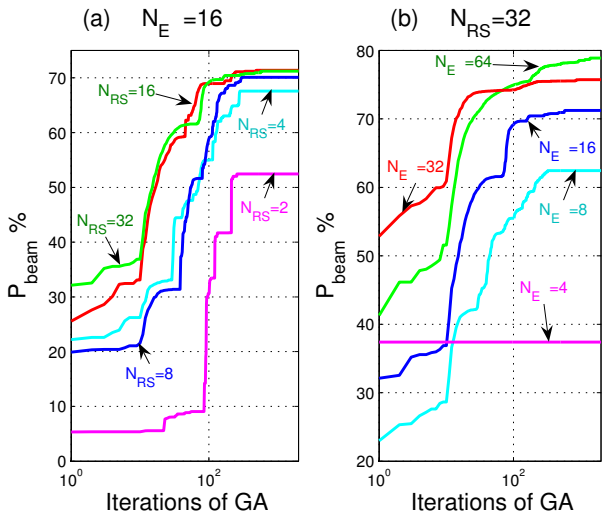

Fig. 11. Convergence of the genetic algorithm for patch array for (a) $N_E = 16$ and varying N_{RS}, and (b) $N_{RS} = 32$ and varying N_E for planar patch structure

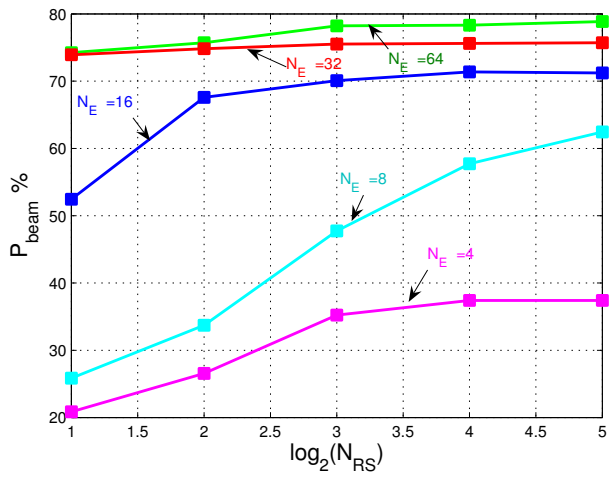

Fig. 12. Beamforming fitness for Patch Array for increasing N_E and N_{RS}

that were simulated for this structure. Saturation of the final performance with respect to N_E and N_{RS} is clearly evident at $N_E = 32$ which is approximate 6 elements per wavelength. However, like the parasitic array, for lower values of of N_E, adding more reconfigurable elements seems to have a stronger benefit on performance than increasing N_{RS}, which is reasonable since in this regime the spatial sampling is low, and adding REs allows the spatial degrees of freedom of the aperture to be better exploited. The apparently low position of the $N_E = 8$ curve is somewhat surprising, and may simply be due to a poor choice of the configuration for that level of complexity. In this case, increasing N_{RS} provides much more dramatic performance increase than the other cases, suggesting that a larger N_{RS} can possibly compensate for a poor arrangement of the REs.

V. Conclusion

This work has reviewed the concept of reconfigurable aperture (RECAP) antennas, focusing on the role of complexity in determining the potential performance of such structures. Complexity in this work was defined in terms of the number of reconfigurable elements (N_{RE}) and reconfigurable states (N_{RS}). Two different RECAP structures were considered, and in each case a point of diminishing returns near 6 elements REs per wavelength was observed. Additionally, we found that performance saturates between $N_{RS} = 4$ and 8 states, suggesting that having many simple REs (where the aperture is better sampled) is more important than having fewer REs with more possible states. Finally, it was observed that even in the region of saturated performance, added complexity can be beneficial in terms of the convergence rate of the genetic algorithm, indicating that higher complexity may be favorable for real-time implementation of RECAP architectures.

References

[1] B. A. Cetiner, H. Jafarkhani, Jiang-Yuan Qian, Hui Jae Yoo, A. Grau, and F. De Flaviis, "Multifunctional reconfigurable MEMS integrated antennas for adaptive MIMO systems," *IEEE Communications Magazine*, vol. 42, pp. 62–70, Dec. 2004.

[2] G. H. Huff, J. Feng, Shenghui Zhang, G. Cung, and J. T. Bernhard, "Directional reconfigurable antennas on laptop computers: Simulation, measurement and evaluation of candidate integration positions," *IEEE Trans. Antennas Propag.*, vol. 52, pp. 3220–3227, Dec. 2004.

[3] Symeon Nikolaou, R. Bairavasubramanian, Jr. Lugo, C., I. Carrasquillo, D. C. Thompson, G. E. Ponchak, J. Papapolymerou, and M. M. Tentzeris, "Pattern and frequency reconfigurable annular slot antenna using PIN diodes," *IEEE Trans. Antennas Propag.*, vol. 54, pp. 439–448, Feb. 2006.

[4] J. L. Freeman, B. J. Lamberty, and G. S. Andrews, "Optoelectronically reconfigurable monopole antenna," *Electronics Letters*, vol. 28, pp. 1502–1503, July 1992.

[5] D. E. Anagnostou, Guizhen Zheng, M. T. Chryssomallis, J. C. Lyke, G. E. Ponchak, J. Papapolymerou, and C. G. Christodoulou, "Design, fabrication, and measurements of an RF-MEMS-based self-similar reconfigurable antenna," *IEEE Trans. Antennas Propag.*, vol. 54, pp. 422 – 432, Feb. 2006.

[6] R. Harrington, "Reactively controlled directive arrays," *IEEE Trans. Antennas Propag.*, vol. 26, pp. 390–395, May 1978.

[7] R. Schlub, D. V. Thiel, J. W. Lu, and S. G. O'Keefe, "Dual-band six-element switched parasitic array for smart antenna cellular communications systems," *Electronics Letters*, vol. 36, pp. 1342–1343, Aug. 2000.

[8] R. Vaughan, "Switched parasitic elements for antenna diversity," *IEEE Trans. Antennas Propag.*, vol. 47, pp. 399–405, Feb. 1999.

[9] J. H. Schaffner, R. Y. Loo, D. F. Sievenpiper, F. A. Dolezal, G. L. Tangonan, J. S. Colburn, J. J. Lynch, J. J. Lee, S. W. Livingston, R. J. Broas, and M. Wu, "Reconfigurable aperture antennas using RF MEMS switches for multi-octave tunability and beam steering," in *Proc. 2000 IEEE Antennas and Propag. Society Intl. Symp.*, Salt Lake City, UT, July 16-21, 2000, vol. 1, pp. 321–324.

[10] L. N. Pringle, P. H. Harms, S. P. Blalock, G. N. Kiesel, E. J. Kuster, P. G. Friederich, R. J. Prado, J. M. Morris, and G. S. Smith, "A reconfigurable aperture antenna based on switched links between electrically small metallic patches," *IEEE Trans. Antennas Propag.*, vol. 52, pp. 1434–1445, June 2004.

[11] D. S. Linden, "Evolving antennas in-situ," *Soft Computing - A Fusion of Foundations, Methodologies and Applications*, vol. 5, pp. 1432–7643, Apr. 2004.

[12] C. M. Coleman, E. J. Rothwell, J. E. Ross, and L. L. Nagy, "Self-structuring antennas," *IEEE Antennas and Propagation Magazine*, vol. 44, pp. 11–23, June 2002.